RESEARCH ARTICLE | FEBRUARY 21 2025

Propulsion contribution from individual filament in a flagellar bundle $\ensuremath{ igoplus}$

Jin Zhu ⑩ ; Yateng Qiao; Lingchun Yan; Yan Zeng; Yibo Wu; Hongyi Bian ⑩ ; Yidi Huang; Yuxin Ye; Yingyue Huang; Russell Ching Wei Hii; Yinuo Teng ⑩ ; Yunlong Guo ⑩ ; Gaojin Li ➡ ⑩ ; Zijie Qu ➡ ⑩



Appl. Phys. Lett. 126, 073702 (2025) https://doi.org/10.1063/5.0243416





Articles You May Be Interested In

Bio-inspired in silico microswimmer: Run and tumble kinematics

Physics of Fluids (March 2023)

A novel computational approach to simulate microswimmers propelled by bacterial flagella

Physics of Fluids (November 2021)

Biotemplated flagellar nanoswimmers

APL Mater. (November 2017)





Propulsion contribution from individual filament in a flagellar bundle

Cite as: Appl. Phys. Lett. **126**, 073702 (2025); doi: 10.1063/5.0243416 Submitted: 10 October 2024 · Accepted: 31 January 2025 · Published Online: 21 February 2025







Jin Zhu, Dateng Qiao, Lingchun Yan, Yan Zeng, Yibo Wu, Hongyi Bian, Dayidi Huang, Yuxin Ye, Yingyue Huang, Russell Ching Wei Hii, Yinuo Teng, Dayunlong Guo, Daojin Li, 2, Dand Zijie Qu^{1, a)}

AFFILIATIONS

¹UM-SJTU Joint Institute, Shanghai Jiao Tong University, Shanghai 200240, People's Republic of China ²State Key Laboratory of Ocean Engineering, School of Ocean and Civil Engineering, Shanghai Jiao Tong University, Shanghai 200240, People's Republic of China

ABSTRACT

Flagellated microorganisms overcome the low-*Reynolds*-number time reversibility by rotating helical flagella [E. M. Purcell, Am. J. Phys. **45**, 3–11 (1977); D. Bray, Cell Movements: From Molecules to Motility, 2nd ed. (Garland Publishing, New York, NY, 2001); Lauga and Powers, Rep. Prog. Phys. **72**, 096601 (2009); and E. Lauga, Annu. Rev. Fluid Mech. **48**, 105–130 (2016)]. For peritrichous bacteria, the randomly distributed flagellar filaments align in the same direction to form a bundle, facilitating complex locomotive strategies [Berg and Brown, Nature **239**, 500–504 (1972); Turner *et al.*, J. Bacteriol. 182, 2793–2801 (2000); and Darnton *et al.*, J. Bacteriol. 189, 1756–1764 (2007)]. To understand the process of flagellar bundling, especially propulsion force generation, we develop a multi-functional macroscopic experimental system and employ advanced numerical simulations for verification. Flagellar arrangements and phase differences between helices are investigated, revealing the variation in propulsion contributions from individual helices. Numerically, we build a time-dependent model to match the bundling process and study the influence of hydrodynamic interactions. Surprisingly, it is found that the total propulsion generated by a bundle of two filaments is constant at various phase differences between the helices. However, the difference between the propulsion from each helix is significantly affected by a phase difference, and only one of the helices is responsible for the total propulsion when the phase difference is equal to π. Building on our experimental and computational results, we develop a theoretical model considering the propulsion contribution of each filament to better understand microbial locomotion mechanisms, especially the wobbling behavior of the cell. Our work also sheds light on the design and control of artificial microswimmers.

Published under an exclusive license by AIP Publishing. https://doi.org/10.1063/5.0243416

Microorganisms navigate complex aquatic environments by beating flexible cilia or rotating rigid helical flagella. Understanding the swimming strategies of various cells at low-*Reynolds*-number environments is crucial for revealing underlying biological processes such as surface colonization, tissue invasion, and escape from harmful substances, and it is also essential to design artificial microswimmers with potential engineering applications. 5-9

During the past few decades, the swimming behavior of *Escherichia coli*, a typical peritrichous bacterium, has been extensively studied. Berg and Brown were pioneers in using a three-dimensional (3D) real-time tracking microscope to study the motion of wild-type *E. coli*, characterized by a "run-and-tumble" behavior. During the "run" phase, *E. coli* cells align their randomly distributed flagellar filaments in the same direction to form a bundle. They then unbundle and change direction during the "tumble" phase by rotating their motor(s) in the opposite direction. ^{10–13}

Numerous studies have been conducted to understand the complex interactions of flagella from various perspectives. For instance, Turner et al. 12 and Darnton et al. 13 employed fluorescently labeled bacteria to visually demonstrate the flagellar bundling process. Kim et al. 14 conducted macroscopic experiments using scaled models to show that the bundling process is a mechanical phenomenon induced by hydrodynamic interactions. Recently, Lim et al. 15 utilized a centimeter-scale multi-flagellated robot to further explore the bundling sequence. Additionally, many numerical studies have been performed, 16,17 including those considering the polymorphic transformations of flagella.¹² Lim and Peskin¹⁸ applied the immersed boundary method, demonstrating that bundling occurs when both flagella are left-handed helices turning counterclockwise (viewed from the nonmotor end looking back toward the motor) or when both are righthanded helices turning clockwise. Lee et al. 17 employed Kirchhoff rod theory to analyze the polymorphic transformations during the flagellar

^{a)}Authors to whom correspondence should be addressed: gaojinli@sjtu.edu.cn and zijie.qu@sjtu.edu.cn

bundling and unbundling process. Previous theoretical studies, such as those done by Buchmann *et al.*¹⁹ and Tatulea-Codrean and Lauga, ²⁰ have explored the influence of phase differences on the hydrodynamics of rotating helices, providing insights into the hydrodynamic interactions and synchronization mechanisms in flagellar bundling dynamics.

Historically, most experimental and theoretical models have treated the flagellar bundle as a single helix. 11,21-26 However, recent studies on motor torque re-allocation among flagella 27 and synchronization of flagella 28-31 have revealed significant differences in the contributions of individual helices during the bundling process. Additionally, little research has focused on propulsion during the "tumble" phase or the flagellar bundling process itself. Overall, a comprehensive study of propulsion generation from individual flagellar filaments and the total propulsion produced by a fully formed bundle is still lacking.

In this work, we conduct an experimental study using a scaled model and directly measure the propulsive force during the bundling process of two helices rotating at constant speeds. Our results indicate that the total propulsion decreases as the helices bundle, primarily due to hydrodynamic interactions. These findings are corroborated by a computational framework that employs a solid–fluid coupled system. Additionally, we observe that while the phase difference between the helices does not alter the total propulsion, it significantly affects the force distribution, with one helix generating almost all the propulsion

when the phase difference is π radians. This result provides an explanation for the cell precession (wobble phenomenon) and is further supported by our theoretical analysis. Contrary to several existing studies, 26,32,33 our results suggest a positive correlation between the swimming speed of the cell and the wobbling effect. We also propose that our findings can inform control strategies for artificial helical swimmers: by adjusting the phase difference between two helices, a perpendicular side force can be generated relative to the swimming direction, which could help navigate complex environments.

The impact of the separation distance between the two helices, denoted as c, and the phase difference ($\Delta\Phi=\Phi_1-\Phi_2$) on the bundling dynamics and propulsive force generation is thoroughly investigated. All experiments are conducted using the multi-functional macroscopic experimental system, as shown in Fig. 1(a) (for details, see supplementary material, Sec. S1). It is important to note that $\Delta\Phi$ remains constant throughout each experiment because the motor operates at a constant speed, providing a simplified approximation of the conditions found in E. coli cells. $^{12,32,34-37}$

First, simple bundling experiments are conducted. The process, documented in supplementary material, Movie S1, aligns with previous studies. ^{14,38} In these experiments, we monitor the propulsion force exerted by each helix during the bundling process, with results shown in Figs. 1(c) and 1(d). The time variable (t) is scaled as $t^* = \omega t/2\pi$, and all propulsion forces (*F*) are scaled as $F^* = F/\mu\omega RL$, where μ , L,

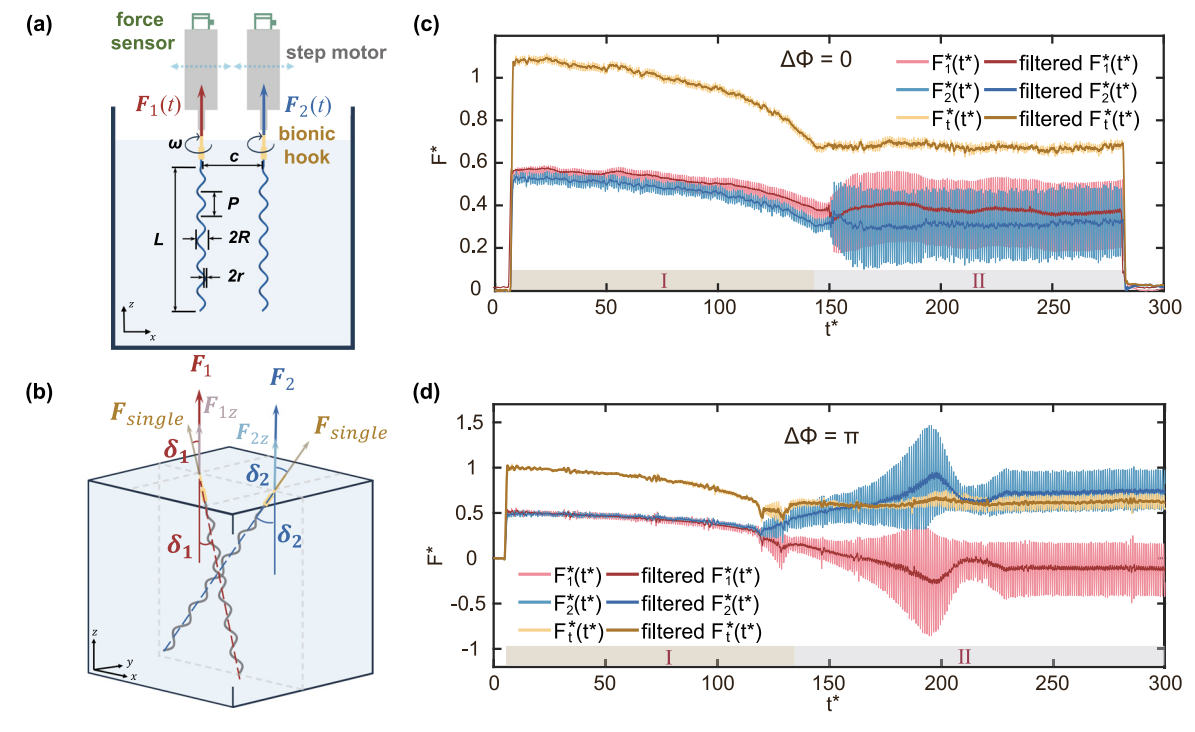


FIG. 1. (a) Illustration of the macroscopic experimental system from the front view. (b) Diagram showing the inclination angle (δ_i) , the preconditioned single-helix propulsion force (F_{single}) , and the propulsion force excluding hydrodynamic interaction $(F_{i,z} = F_{\text{single}} \cos(\delta_i))$ during the bundling process, where i=1 and 2 correspond to each helix. (c) and (d) Measured propulsion force trends during the bundling process with a fixed separation distance (c=73.6 mm) and two phase differences $(\Delta \Phi = 0 \text{ and } \Delta \Phi = \pi)$. The figures depict the trends in the scaled forces $F_1^*(t^*)$, $F_2^*(t^*)$, and $F_l^*(t^*)$ over scaled time (t^*) . Thinner lines represent the raw data for $F_1^*(t^*)$, $F_2^*(t^*)$, and $F_l^*(t^*)$, while thicker lines show the filtered data, highlighting the effect of removing the rotational speed frequency (ω) . The helices bundling process exhibits two distinct states: a bundling state (state I) and a steady state (state II). The shaded bars with different colors above the horizontal axis indicate these distinct states.

 ω , and R represent fluid viscosity, helix length, rotation speed, and helical radius, respectively (for details, see supplementary material, Sec. S1). The sensor measures force solely along the axial (z) direction, as illustrated in Fig. 1(b).

An overall decaying trend in the force generated by each helix over time $[F_1^*(t^*)]$ and $F_2^*(t^*)]$ is observed, starting with an initial value of $F_{initial}^* \approx 0.5$. This is consistent with predictions from traditional resistive force theory (RFT)^{22,39} for a single immersed helix at low *Reynolds* number (see supplementary material, Sec. S2.A.1) and the single-helix propulsion force experiment (see supplementary material, Sec. S2.A.3). In Figs. 1(c) and 1(d), both cases show a similar overlap between the force–time curves from each helix, indicating system symmetry. When we examine the total propulsion force $F_t^*(t^*)$, it is clear that the force plateaus at $T_b^* \approx 140$, when the two helices contact each other and cease bundling (also detailed in supplementary material, Sec. S2.A.4 and supporting Video 1, with clear labeling of different states). Here, T_b^* is defined as the dimensionless bundling time of the system, scaled by $T_b^* = \omega T_b/2\pi$. We categorize the experiment into two phases: a

bundling state ($t^* < T_h^*$) and a steady state ($t^* > T_h^*$). In Figs. 1(c) and 1(d), the total propulsion, $F_t^*(t^*) = F_1^*(t^*) + F_2^*(t^*)$, represented by a yellow curve, is initially about twice the value of propulsion generated by a single helix ($F_{\mathrm{single}}^* \approx 0.5$),which is the preconditioned single-helix propulsion force obtained in the single-helix test as described in supplementary material, Sec. S2.A.3. The initial stage of the helices bundling process exhibits minimal interaction between the velocity fields generated by the two helices. As time progresses, $F_t^*(t^*)$ changes due to the helix tilt and increased hydrodynamic interaction. In the steady state, the fluctuation of $F_t^*(t^*)$ is considerably smaller than that of $F_1^*(t^*)$ and $F_2^*(t^*)$, which is attributable to helix collisions. However, Fig. 1(d) also shows that, in the case of $\Delta\Phi = \pi$, $F_1^*(t^*)$ and $F_2^*(t^*)$ still vary for some time before reaching a constant value, even though $F_t^*(t^*)$ becomes constant in the steady state ($t^*>T_b^*$). The consistent behavior of $F_t^*(t)$ and the varying behavior of $F_1^*(t^*)$ and $F_2^*(t^*)$ for individual helices are also attributed to hydrodynamic interaction, as discussed later.

Further examination of the cause of the propulsion change focuses on the inclination of each helix at steady state. As Fig. 1(b)

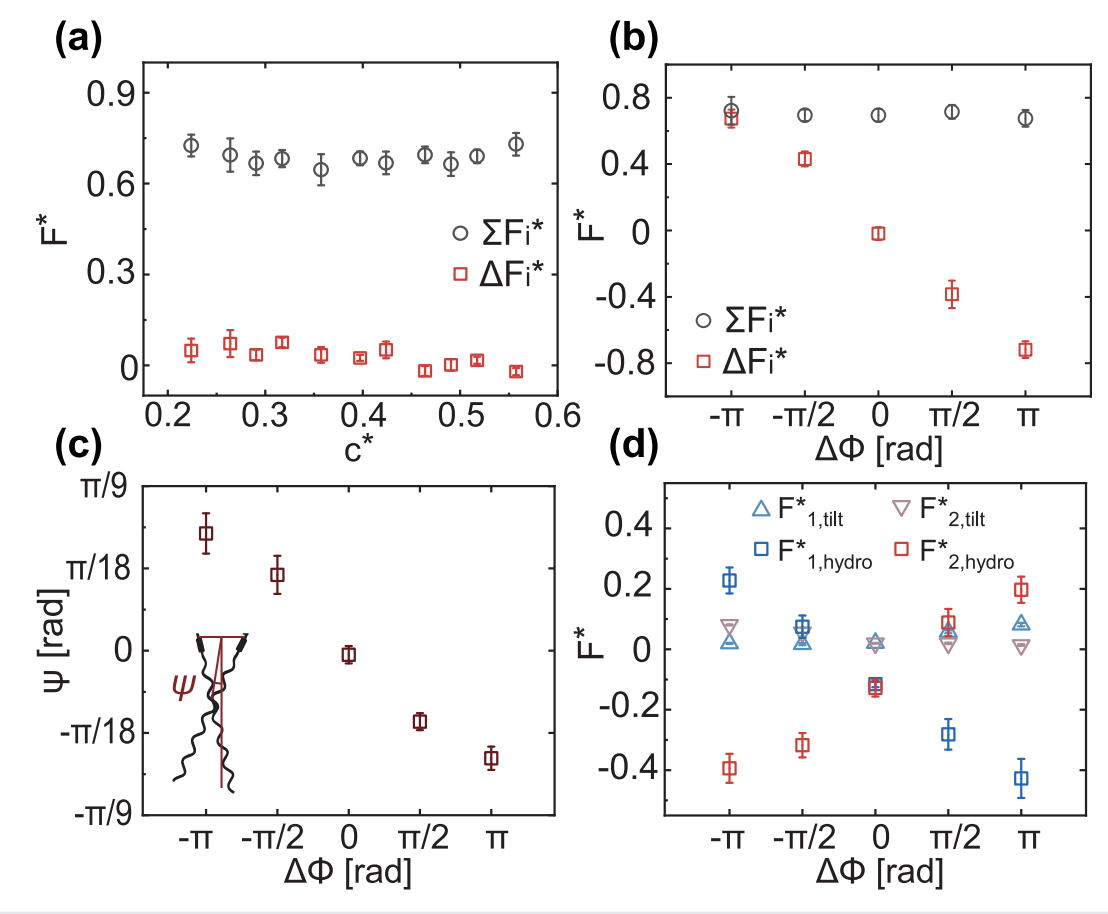


FIG. 2. Influence of separation distance (c^*) and phase difference $(\Delta\Phi)$ on the steady-state bundling system. (a) Scaled force summation (ΣF_i^*) and difference (ΔF_i^*) as a function of separation distance (c^*) with $\Delta\Phi=0$. Each data point represents 15 independent measurements taken over more than 30 s in the steady state of the bundling process. (b) Scaled force summation (ΣF_i^*) and difference (ΔF_i^*) as a function of phase difference $(\Delta\Phi)$. (c) Leaning angle (ψ) is defined as the small angle between the z-axis and the line connecting the intersection of the help summation in propulsion due to the tilt of the system $(F_{i,tilt}^*)$ and due to the hydrodynamic interaction $(F_{i,hydro}^*)$ under conditions of different $\Delta\Phi$. The values of separation distance (c^*) from (b) to (d) is 0.49. Each data point in (b) to (d) represents ≥ 5 independent measurements taken over more than 30 s in the steady state of the bundling process.

shows, the inclination angle δ_i (where i=1 and 2 for each helix) is defined as the small angle between the z-axis and the helix in the steady state. The z-component of the propulsion force in the absence of interactions with the other helix is defined as $F_{i,z}^* = F_{single}^* \cos(\delta_i)$. The difference between F_i^* and $F_{i,z}^*$ is mainly attributed to the hydrodynamic interaction induced by the existence of the other helix in the system $(F_{i,hydro}^* = F_i^* - F_{i,z}^*)$. Here, we define the reduction in propulsion due to the tilt of the system as $F_{tilt}^* = F_{single}^* - F_{i,z}^*$. For example, in the case of $\Delta\Phi = 0$, $F_{i,z}^* = 0.48$ and $F_{i,hydro}^*$ is about -0.12. However, $F_{tilt}^* = -0.02$, is significantly less impactful than the hydrodynamic interaction. Also, as shown in Fig. 1(d), the case of $\Delta\Phi = \pi$ breaks the symmetry of the bundling system, indicating a greater influence of hydrodynamic interaction since the two individual helices show a large force difference in the steady state. This indicates that the primary factor in the propulsion variation during the bundling process is the hydrodynamic interaction.

Peritrichous bacteria, such as *E. coli, Bacillus subtilis*, and *Proteus mirabilis*, possess multiple flagella that project in various directions. ^{11,12,40-43} Variations in cell body shape and the random anchoring of the motors ^{11,40-43} cause the flagella separation distances to vary widely. Understanding the dynamics of flagellar bundling across different separation distances is therefore essential. Our experimental setup, constrained by mechanical limitations, allows us to adjust the separation distance ratio $c^* = c/L$ from 0.22 to 0.56, enabling us to test a wider range of separation distances.

First, the measured bundling time (T_b) is investigated [see supplementary material, Fig. S12(a)]. T_b^* increases nonlinearly with c^* , which partly explains the significant variation in bundling times reported in previous studies. Additionally, the total propulsion ΣF_i^* in the steady state is investigated [see Fig. 2(a)]. Interestingly, ΣF_i^* remains

constant regardless of c^* , suggesting that for a fixed number of flagellar filaments (two in this case), the propulsion is constant. Moreover, in the steady state, the included angles between the helices remain identical across different c^* , [see supplementary material, Fig. S12(b)]. This, combined with the symmetry of the system, results in identical inclination angles δ_i .

Furthermore, we studied the effect of phase difference ($\Delta\Phi$) on propulsion. In Fig. 2(b), ΣF_i^* is plotted over various values of $\Delta\Phi$, ranging from $-\pi$ to π with an interval of $\pi/2$. While ΣF_i^* remains constant across different $\Delta\Phi$, the difference in propulsion, $\Delta F_i^* = F_1^* - F_2^*$, generated by each helix is linearly correlated with $\Delta\Phi$. Remarkably, at $\Delta\Phi = -\pi$, ΔF_i^* approximates ΣF_i^* , indicating that the total propulsion is contributed by only one filament. This finding holds for $\Delta\Phi = \pi$ as well, by comparing $-\Delta F_i^*$ with ΣF_i^* due to symmetry.

What causes the propulsion difference? It is noted that with varying $\Delta\Phi$, the system loses symmetry, causing the bundle to lean toward the helix with a lagging phase at the steady state, as shown in Fig. 2(c). The leaning angle, ψ , is plotted over different values of $\Delta\Phi$. Consequently, the inclination angle, δ_i , is no longer identical for the helices in the steady state (see supplementary material, Table S2). The propulsion excluding hydrodynamic interaction, F_{iz}^* is calculated and plotted over $\Delta\Phi$ in Fig. 2(d). However, the propulsion difference calculated without considering the hydrodynamic interaction is significantly smaller than that measured directly from the sensor [Fig. 2(d), square markers]. Thus, the altered hydrodynamic interaction is identified as the primary cause of the difference in propulsion between each helix, with this effect increasing with $\Delta\Phi$.

To further elucidate the hydrodynamic interaction, we conduct a numerical simulation using a solid-fluid coupled solver implemented

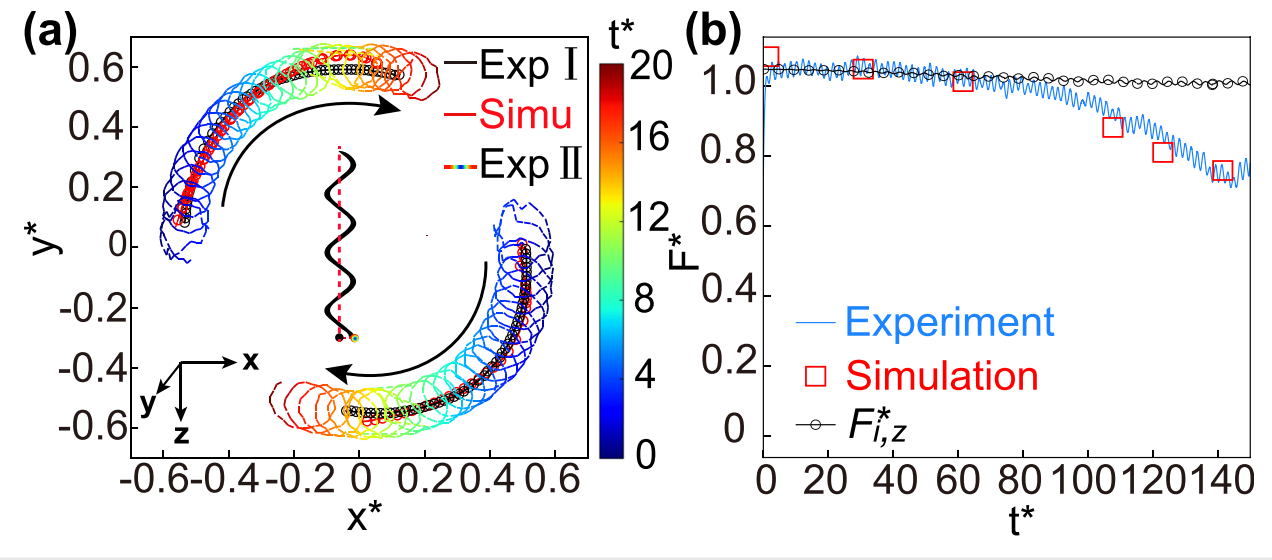


FIG. 3. Comparison between simulation results and experimental results. (a) Comparison of flagella tail trajectories between simulation and experiment with a fixed separation distance ($c^* = 0.264$, $\Delta \Phi = 0$). The red line represents the simulation trajectory of the central point of the helix, shown as the black point in the inset figure; the black line represents the experimental trajectory of the tentral point of the helix, shown as the gradient-colored line represents the experimental trajectory of the tip of the helix, shown as the gradient color point in the inset figure. The position of x and y are scaled as $x^* = x/L$ and $y^* = y/L$, respectively. (b) Comparison among experiment, simulation, and theoretical results of total propulsion force as a function of time (t^*) with fixed separation distance ($c^* = 0.49$, $\Delta \Phi = 0$). Theoretical propulsion force is calculated by $F^*_{i,z} = F^*_{single} \cos(\delta_i)$, where F^*_{single} is the single flagella numerical propulsion (see the supplementary material, Fig. S16). Here, $\Sigma F^*_{i,z}$ represents the summation of theoretical propulsion force.

in OpenFOAM (see supplementary material, Sec. S2.B). The accuracy of the numerical solver is validated by simulating the motion of a Jeffery Orbit⁴⁵ (supplementary material, Sec. S2.B.3) and the propulsion generated by a single helix (supplementary material, Sec. S2.B.5), with results consistent with theoretical predictions.⁴⁶ In the simulations, each helix is modeled as a rigid body rotating around a fixed point at a constant speed, with boundary conditions, fluid properties, and initial conditions replicating those of the experimental setup.

The bundling process observed in the simulation aligns with the experimental observations in Fig. 3(a), further confirming the simulation's accuracy. Additionally, the propulsion values calculated from the simulation [Fig. 3(b)] closely match the experimental results. To visualize the interaction directly, we plot the flow field from the simulation at various time points during the bundling process in Figs. 4(a)-4(c).

At $t^*=1$, the flow field resembles the superposition of two distinct helices. The velocity near the field's origin, which is the center of the system, is nearly zero. By $t^*=30$, it appears that the flow fields generated by each helix begin to extend into the area occupied by the other helix. Consequently, the velocity near the origin increases. However, the propulsion measured from each helix remains similar to that observed without considering the hydrodynamic interactions between the helices, as shown in Fig. 3(b) with black markers. At $t^*=60$, we have observed a subtle difference in propulsion, as indicated in Fig. 3(b). The velocity between the helices also intensifies as they bundle closer together, indicating stronger hydrodynamic interactions. The radial decay of the flow velocity U^* at different times indicates the different bundling stages [Fig. 4(d)]. The velocity peak value becomes larger and the radius becomes smaller as time increases, indicating the

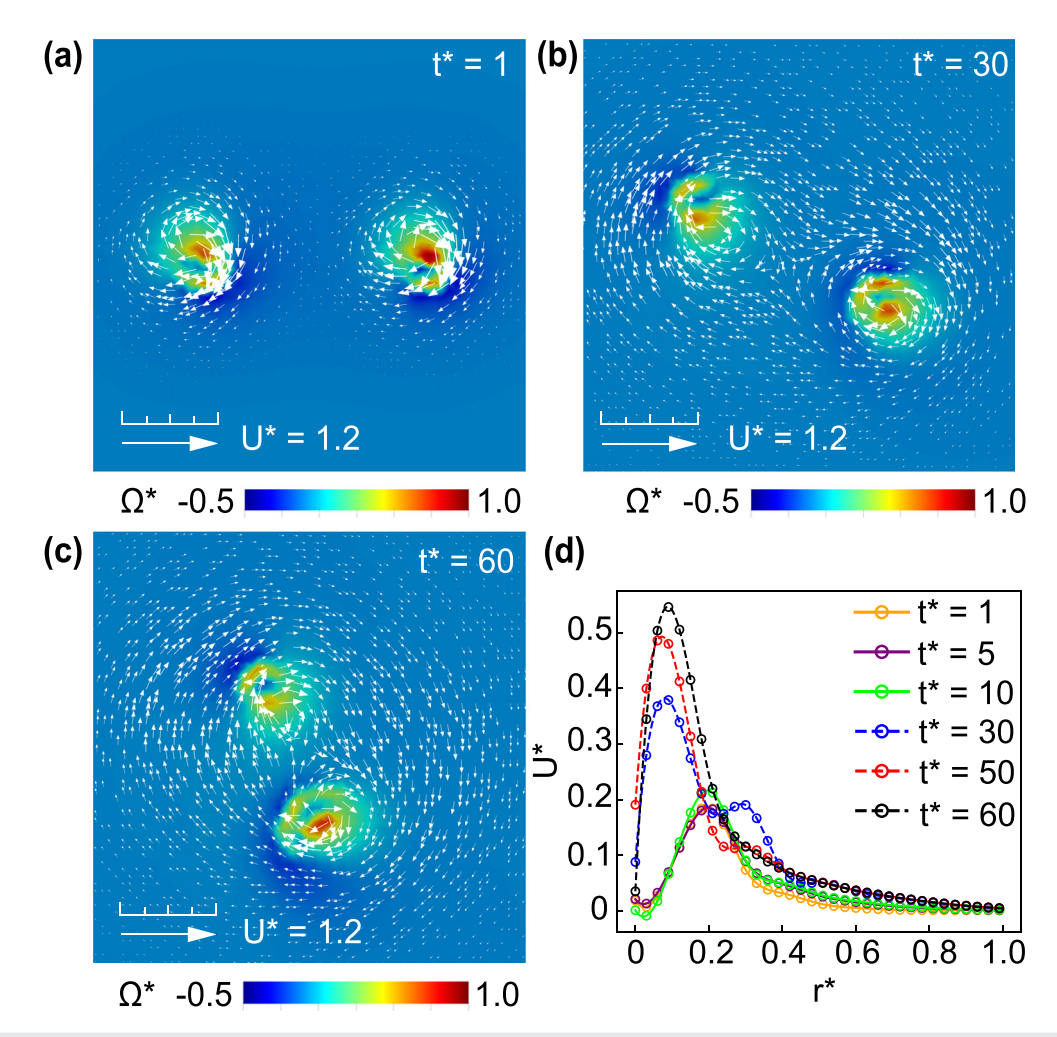


FIG. 4. Flow field at instantaneous times during the bundling process ($c^*=0.49, \Delta\Phi=0$). The z-plane is set at the plane of $z^*=1$, where $z^*=z/L$. $z^*=0$ is defined at the proximal end of the helix, near the bionic hook. (a)–(c) Vorticity field with instantaneous velocity field at different times. It is noted that the velocity fields selected at these three times correspond to the first three simulation data point in Fig. 3(b). The vorticity in the flow field is scaled as $\Omega^*=\Omega/\Omega_{max}$, where Ω_{max} is the max vorticity at each instantaneous t^* . The length of the arrows represent the magnitude of the fluid velocity, while the direction of the arrows indicates the direction of fluid flow. The legend shows the velocity magnitude as represented by the color scale. (d) Radial decay of the flow velocity U^* at each instantaneous t^* , with $r^*=0$ corresponding to the center of the fluid field, $r^*=0.2$ corresponding to the flagella rotation axis. Here, U^* is scaled as $U^*=U/(\omega R)$, where U is the instantaneous velocity magnitude. The selection of the coordinate system is designed to neutralize the effect of different θ values, focusing solely on U^* as a function of r^* .

bundling process. In the beginning, the velocity peak is located near $r^* = 0.2$ (denoted by the curves $t^* = 1$, $t^* = 5$, $t^* = 10$), where the flow velocity is locally induced by each helix. As time progresses, the interaction between the velocity fields induced by two helices gradually increases. This process is what we call the bundling process. This interaction caused a double peak to appear at $t^* = 30$. When the two helices come closer together, the double peak disappears and a single peak appears near the center of the system, indicating a stronger interaction between the velocity fields. The correlation coefficient of the velocity field is also shown in supplementary material, Sec. S2.E (see supplementary material, Fig. S20). Moreover, the tendency of the helices to lean toward one during the steady state is attributed to a hydrodynamic force acting along the x-axis. This phenomenon is well demonstrated in the simulation results (supplementary material, Sec. S2.D), where the side force acting on the system is shown for cases where the phases are either $\Delta \Phi = 0$ [see supplementary material, Fig. S18(a)] or $\Delta\Phi = \pi$ [see supplementary material, Fig. S18(b)].

Previous studies have observed a "wobbling" phenomenon in flagellated bacteria swimming, attributed to the misalignment between the bacterium's body axis and the bundle axis. 13,24,47,48 However, the relationship between the wobbling effect and the swimming speed has yet to be clarified. 13,26,32,33,49 In our study, the varied leaning angles (ψ) resulting from different phase differences ($\Delta\Phi$) also suggest potential misalignment. However, is misalignment the sole reason for the wobbling behavior? To explore this, we conduct a simple theoretical analysis by modeling the cell body as a two-dimensional (2D) ellipsoid with the major axis length $(a = 2.5 \,\mu\text{m})$ and the minor axis length $(b = 1 \,\mu\text{m})$. The uneven propulsion is modeled as two pairs of point forces $(F_1^{\parallel}, F_1^{\perp})$ and $F_2^{\parallel}, F_2^{\perp})$ acting on the ellipse, illustrated in supplementary material, Fig. S21. The angles δ_1 and δ_2 are defined similarly but in a 2D plane, with $F_i^{\perp} = F_i^{\parallel} \tan \delta_i$. It is noted that the δ_i values used here are measured from macroscopic experimental results, establishing a connection between macroscopic observations and theoretical analysis in our study. Details are provided in supplementary material, Table S2.

Building on previous research, 26,47 it is suggested that the wobbling frequency is equal to the self-rotating frequency of the cell body, implying that the relative angle of the bundle axis to the body axis remains constant during the "run" phase. Given the force-free nature of micro-swimmers in low-*Reynolds*-number environments, 11,50 a force balance analysis is essential. This analysis focuses on the angle β , which is equal to half of the wobble angle and is represented in the swimming direction relative to the body's major axis (see supplementary material, Fig. S21). 13

With the given geometry of the cell body, a constant drag force in the z-direction, the propulsion force ratio Λ , and the inclination angle δ_i of each flagellum, the wobble angle 2β and swimming speed V are calculated using the principle of force equilibrium in two directions. The results are summarized in Table I, with detailed force equilibrium calculations provided in supplementary material, Sec. S2.G. The ratio

TABLE I. Magnitude of cell speed (V) and wobble angle (2β) with different Λ .

Λ	1/35	1/5	1	4	68
V (μm/s)	44	41	40	41	43
2β (°)	24.83	13.17	0.36	12.11	21.73

 $\Lambda = F_2^{\parallel}/F_1^{\parallel}$ and the inclination angle δ_i are used to incorporate our macroscopic experimental results into the theoretical model analysis. In these calculations, the drag force in the z-direction $(F_{drag}^{\parallel}=F_{1}^{\parallel}+F_{2}^{\parallel}=0.24 \text{ pN})$ from the no-wobble case, where $\Lambda=1$, is treated as a constant. This assumption aligns with our macroscopic experimental findings, which show that the total propulsion force ΣF_i is minimally affected by variations in separation distance c and phase difference $\Delta\Phi$. The results corroborate the values measured in previous studies, 13,26,48 and intriguingly, we observe a positive correlation between the swimming speed V and the wobble angle, supporting the findings by Liu et al. 49 Contrary to their explanation of additional propulsion generated by cell body rotation due to an asymmetric body shape, our findings suggest an enhancement in swimming speed even with an axisymmetric cell body, primarily due to the significant force imbalance between each helix, which not only increases the wobbling effect but also contributes to higher propulsion and faster swimming.

In this study, a macroscopic experimental system was employed to investigate the bundling dynamics of two helices rotating at constant speeds, with a focus on the changes in propulsion during the bundling process. We discovered that the phase difference between the helices leads to significant deviations in propulsion in the steady state, while the total propulsion remains unchanged. Our experimental findings, supported by numerical simulations, highlight the crucial role of hydrodynamic interactions in both the bundling process and propulsion generation.

Additionally, theoretical analysis revealed that differences in helical propulsion could induce wobbling in the cell, and that the swimming speed is positively correlated with the wobbling effect. This observation suggests a potential control strategy for helical microswimmers: By generating a lateral force in a two-helix system, it may be possible to alter the swimming direction without needing to modify the source of propulsion, such as an external magnetic field.

However, our findings are limited to a system involving two constant-speed helices in a Newtonian fluid and a simplified 2D theoretical framework. Further research works and a more comprehensive theory are required to fully understand the complex interactions among multiple flagella in non-Newtonian fluids.

See the supplementary material for more details on materials and methods, data analysis, experimental results, and numerical methods.

We thank Shuo Guo and Hepeng Zhang for offering many useful comments to revise the paper. This work was funded by the NSFC (Grant Nos. 12202275, 12372264, and STCSM 22YF1419800) and the Natural Science Foundation of Shanghai (Grant No. 23ZR1430800).

AUTHOR DECLARATIONS Conflict of Interest

The authors have no conflicts to disclose.

Author Contributions

Jin Zhu and Yateng Qiao contributed equally to this work.

Jin Zhu: Conceptualization (equal); Data curation (equal); Formal analysis (equal); Investigation (equal); Methodology (equal);

Visualization (equal); Writing - original draft (equal). Yateng Qiao: Conceptualization (supporting); Data curation (equal); Formal analysis (equal); Investigation (equal); Methodology (equal); Visualization (equal); Writing - original draft (equal). Lingchun Yan: Formal analysis (equal); Investigation (equal); Methodology (equal); Validation (equal). Yan Zeng: Formal analysis (equal); Investigation (equal); Methodology (equal). Yibo Wu: Formal analysis (equal); Investigation (equal); Methodology (equal). Hongyi Bian: Investigation (equal); Software (lead). Yidi Huang: Formal analysis (equal); Investigation (equal); Software (supporting). Yuxin Ye: Formal analysis (equal); Investigation (equal); Software (supporting). Yingyue Huang: Formal analysis (equal); Investigation (equal); Software (supporting). Russell Ching Wei Hii: Formal analysis (equal); Investigation (equal); Software (supporting). Yinuo Teng: Resources (equal). Yunlong Guo: Resources (equal). Gaojin Li: Conceptualization (equal); Funding acquisition (equal); Project administration (equal); Resources (equal); Supervision (equal). Zijie Qu: Conceptualization (equal); Funding acquisition (equal); Project administration (equal); Resources (equal); Supervision (equal); Writing - original draft (equal).

DATA AVAILABILITY

The data that support the findings of this study are available from the corresponding authors upon reasonable request.

REFERENCES

- ¹D. Bray, Cell Movements: From Molecules to Motility, 2nd ed. (Garland Publishing, New York, NY, 2001).
- ²K. M. Ottemann and A. C. Lowenthal, "Helicobacter pylori uses motility for initial colonization and to attain robust infection," Infect. Immun. 70, 1984–1990 (2002).
- ³J. A. Horstmann, E. Zschieschang, T. Truschel, J. De Diego, M. Lunelli, M. Rohde, T. May, T. Strowig, T. Stradal, M. Kolbe, and M. Erhardt, "Flagellin phase-dependent swimming on epithelial cell surfaces contributes to productive Salmonella gut colonisation," Cell. Microbiol. 19, e12739 (2017).
- ⁴D. L. Valentine, J. D. Kessler, M. C. Redmond, S. D. Mendes, M. B. Heintz, C. Farwell, L. Hu, F. S. Kinnaman, S. Yvon-Lewis, M. Du, E. W. Chan, F. G. Tigreros, and C. J. Villanueva, "Propane respiration jump-starts microbial response to a deep oil spill," Science 330, 208–211 (2010).
- ⁵L. Zhang, J. J. Abbott, L. Dong, K. E. Peyer, B. E. Kratochvil, H. Zhang, C. Bergeles, and B. J. Nelson, "Characterizing the swimming properties of artificial bacterial flagella," Nano Lett. 9, 3663–3667 (2009).
- ⁶D. Ahmed, T. Baasch, B. Jang, S. Pane, J. Dual, and B. J. Nelson, "Artificial swimmers propelled by acoustically activated flagella," Nano Lett. **16**, 4968–4974 (2016).
- ⁷X. Yan, Q. Zhou, M. Vincent, Y. Deng, J. Yu, J. Xu, T. Xu, T. Tang, L. Bian, Y.-X. J. Wang, K. Kostarelos, and L. Zhang, "Multifunctional biohybrid magnetite microrobots for imaging-guided therapy," Sci. Robot. 2, eaaq1155 (2017).
- ⁸J. Choi, J. Hwang, J. Kim, and H. Choi, "Recent progress in magnetically actuated microrobots for targeted delivery of therapeutic agents," Adv. Healthcare Mater. 10, 2001596 (2021).
- ⁹Y. Deng, A. Paskert, Z. Zhang, R. Wittkowski, and D. Ahmed, "An acoustically controlled helical microrobot," Sci. Adv. 9, eadh5260 (2023).
- ¹⁰H. C. Berg and D. A. Brown, "Chemotaxis in *Escherichia coli* analysed by three-dimensional tracking," Nature 239, 500–504 (1972).
- ¹¹E. Lauga, "Bacterial hydrodynamics," Annu. Rev. Fluid Mech. **48**, 105–130 (2016).
- ¹²L. Turner, W. S. Ryu, and H. C. Berg, "Real-time imaging of fluorescent flagellar filaments," J. Bacteriol. 182, 2793–2801 (2000).
- ¹³N. C. Darnton, L. Turner, S. Rojevsky, and H. C. Berg, "On torque and tumbling in swimming Escherichia coli," J. Bacteriol. 189, 1756–1764 (2007).

- ¹⁴M. Kim, J. C. Bird, A. J. V. Parys, K. S. Breuer, and T. R. Powers, "A macroscopic scale model of bacterial flagellar bundling," Proc. Natl. Acad. Sci. U. S. A. 100, 15481–15485 (2003).
- ¹⁵S. Lim, A. Yadunandan, and M. Khalid Jawed, "Bacteria-inspired robotic propulsion from bundling of soft helical filaments at low Reynolds number," Soft Matter 19, 2254–2264 (2023).
- ¹⁶D. Tong, A. Choi, J. Joo, and M. K. Jawed, "A fully implicit method for robust frictional contact handling in elastic rods," Extreme Mech. Lett. 58, 101924 (2023).
- ¹⁷W. Lee, Y. Kim, B. E. Griffith, and S. Lim, "Bacterial flagellar bundling and unbundling via polymorphic transformations," Phys. Rev. E 98, 052405 (2018).
- ¹⁸S. Lim and C. S. Peskin, "Fluid-mechanical interaction of flexible bacterial flagella by the immersed boundary method," Phys. Rev. E 85, 036307 (2012).
- ¹⁹A. Buchmann, L. J. Fauci, K. Leiderman, E. Strawbridge, and L. Zhao, "Mixing and pumping by pairs of helices in a viscous fluid," Phys. Rev. E 97, 023101 (2018).
- 20M. Tătulea-Codrean and E. Lauga, "Asymptotic theory of hydrodynamic interactions between slender filaments," Phys. Rev. Fluids 6, 074103 (2021).
- ²¹E. Lauga and T. R. Powers, "The hydrodynamics of swimming microorganisms," Rep. Prog. Phys. 72, 096601 (2009).
- ²²G. J. Hancock, "The self-propulsion of microscopic organisms through liquids," Proc. R. Soc. London, Ser. A 217, 96–121 (1953).
- ²³M. Holwill and R. Burge, "A hydrodynamic study of the motility of flagellated bacteria," Arch. Biochem. Biophys. 101, 249–260 (1963).
- ²⁴J. Keller and S. Rubinow, "Swimming of flagellated microorganisms," Biophys. J. 16, 151–170 (1976).
- 25Y. Magariyama and S. Kudo, "A mathematical explanation of an increase in bacterial swimming speed with viscosity in linear-polymer solutions," Biophys. J. 83, 733-739 (2002).
- ²⁶A. E. Patteson, A. Gopinath, M. Goulian, and P. E. Arratia, "Running and tumbling with *E. coli* in polymeric solutions," Sci. Rep. 5, 15761 (2015).
- ²⁷S. Kamdar, D. Ghosh, W. Lee, M. Tătulea-Codrean, Y. Kim, S. Ghosh, Y. Kim, T. Cheepuru, E. Lauga, S. Lim, and X. Cheng, "Multiflagellarity leads to the size-independent swimming speed of peritrichous bacteria," Proc. Natl. Acad. Sci. U. S. A. 120, e2310952120 (2023).
- ²⁸M. Reichert and H. Stark, "Synchronization of rotating helices by hydrodynamic interactions," Eur. Phys. J. E 17, 493–500 (2005).
- 29B. Qian, H. Jiang, D. A. Gagnon, K. S. Breuer, and T. R. Powers, "Minimal model for synchronization induced by hydrodynamic interactions," Phys. Rev. E 80, 061919 (2009).
- ³⁰S. Y. Reigh, R. G. Winkler, and G. Gompper, "Synchronization and bundling of anchored bacterial flagella," Soft Matter 8, 4363 (2012).
- ³¹M. Tătulea-Codrean and E. Lauga, "Elastohydrodynamic synchronization of rotating bacterial flagella," Phys. Rev. Lett. 128, 208101 (2022).
- ³²Z. Qu and K. S. Breuer, "Effects of shear-thinning viscosity and viscoelastic stresses on flagellated bacteria motility," Phys. Rev. Fluids 5, 073103 (2020).
- ³³S. Kamdar, S. Shin, P. Leishangthem, L. F. Francis, X. Xu, and X. Cheng, "The colloidal nature of complex fluids enhances bacterial motility," Nature 603, 819–823 (2022).
- ³⁴R. M. Berry and H. C. Berg, "Absence of a barrier to backwards rotation of the bacterial flagellar motor demonstrated with optical tweezers," Proc. Natl. Acad. Sci. U. S. A. 94, 14433–14437 (1997).
- 35Y. Sowa and R. M. Berry, "Bacterial flagellar motor," Q. Rev. Biophys. 41, 103–132 (2008).
- ³⁶N. Wadhwa, Y. Tu, and H. C. Berg, "Mechanosensitive remodeling of the bacterial flagellar motor is independent of direction of rotation," Proc. Natl. Acad. Sci. U. S. A. 118, e2024608118 (2021).
- ³⁷J. Yuan, K. A. Fahrner, L. Turner, and H. C. Berg, "Asymmetry in the clockwise and counterclockwise rotation of the bacterial flagellar motor," Proc. Natl. Acad. Sci. U. S. A. 107, 12846–12849 (2010).
- ³⁸M. J. Kim, M. J. Kim, J. C. Bird, J. Park, T. R. Powers, and K. S. Breuer, "Particle image velocimetry experiments on a macro-scale model for bacterial flagellar bundling," Exp. Fluids 37, 782–788 (2004).
- ³⁹B. Rodenborn, C.-H. Chen, H. L. Swinney, B. Liu, and H. P. Zhang, "Propulsion of microorganisms by a helical flagellum," Proc. Natl. Acad. Sci. U. S. A. 110, E338–E347 (2013).
- 40"Larger organisms," in *E. coli in Motion*, edited by H. C. Berg (Springer, New York, NY, 2004), pp. 7–17.

- ⁴¹J. Clopés and R. G. Winkler, "Flagellar arrangements in elongated peritrichous bacteria: Bundle formation and swimming properties," Eur. Phys. J. E 44, 17 (2021).

 42J. Najafi, M. R. Shaebani, T. John, F. Altegoer, G. Bange, and C. Wagner,
- "Flagellar number governs bacterial spreading and transport efficiency," Sci. Adv. 4, eaar6425 (2018).
- ⁴³J. Najafi, F. Altegoer, G. Bange, and C. Wagner, "Swimming of bacterium Bacillus subtilis with multiple bundles of flagella," Soft Matter 15, 10029-10034
- 44Z. Qu, F. Z. Temel, R. Henderikx, and K. S. Breuer, "Changes in the flagellar bundling time account for variations in swimming behavior of flagellated bacteria in viscous media," Proc. Natl. Acad. Sci. U. S. A. 115, 1707-1712
- ⁴⁵G. B. Jeffery, "The motion of ellipsoidal particles immersed in a viscous fluid,"
- Proc. R. Soc. London, Ser. A 102, 161-179 (1922).

 46S. Kim and S. J. Karrila, "Chapter 5 resistance and mobility relations," in Microhydrodynamics, edited by S. Kim and S. J. Karrila (Butterworth-Heinemann, 1991), pp. 107-145.
- ⁴⁷Y. Hyon, Marcos, T. R. Powers, R. Stocker, and H. C. Fu, "The wiggling trajectories of bacteria," J. Fluid Mech. 705, 58-76 (2012).
- 48Y. Yin, H.-T. Yu, H. Tan, H. Cai, H.-Y. Chen, C.-J. Lo, and S. Guo, "Escaping
- speed of bacteria from confinement," Biophys. J. 121, 4656–4665 (2022).

 ⁴⁹B. Liu, M. Gulino, M. Morse, J. X. Tang, T. R. Powers, and K. S. Breuer, "Helical motion of the cell body enhances Caulobacter crescentus motility," Proc. Natl. Acad. Sci. U. S. A. 111, 11252-11256 (2014).
- 50 E. M. Purcell, "Life at low Reynolds number," Am. J. Phys. **45**, 3–11 (1977).